Journal of Applied Mathematics and Physics, 2025, 13(4), 1577-1598
https://www.scirp.org/journal/jamp
ISSN Online: 2327-4379
ISSN Print: 2327-4352

Robust Sensitivity Design Optimization to Generalized Systems-Based Theoretical Kinematic Inverse/Regular Wedge Cam Theory for Three-Point Diametral Self-Centering Motion

Shawn P. Guillory, Alan A. Barhorst, Jim Lee, Raju Gottumukkala, Jonathan R. Raush, Terrence L. Chambers

Department of Mechanical Engineering, The University of Louisiana at Lafayette, Lafayette, USA
Email: shawn.guillory1@louisiana.edu, alan.barhorst@louisiana.edu, jim.lee@louisiana.edu, jonathan.raush@louisiana.edu, raju.gottumukkala@louisiana.edu, terrence.chambers@louisiana.edu

How to cite this paper: Guillory, S.P., Barhorst, A.A., Lee, J., Gottumukkala, R., Raush, J.R. and Chambers, T.L. (2025) Robust Sensitivity Design Optimization to Generalized Systems-Based Theoretical Kinematic Inverse/Regular Wedge Cam Theory for Three-Point Diametral Self-Centering Motion. *Journal of Applied Mathematics and Physics*, **13**, 1577-1598.
https://doi.org/10.4236/jamp.2025.134085

Received: March 27, 2025
Accepted: April 24, 2025
Published: April 27, 2025

Abstract

Techniques of robust sensitivity design optimization involving nonlinear interior point algorithms and/or second derivatives are utilized in concert with recently developed generalized robust systems-based theoretical kinematic inverse/regular wedge cam procedures for producing self-centering motion applicable to three-point clamping device design about cylindrical workpieces that vary within a prescribed size range. With the use of the FindMinimum function in Wolfram Mathematica for exploring the specific optimization application to associated product designs in conjunction with computer-aided engineering validation efforts, significantly novel results are revealed related to improving force convergence and stabilization between grippers across the full diametral surface range (on the order of 15 to 10 times respectively) which is highly beneficial for clamping force and contact stress as well as dynamic characteristics including vibration among others. Essentially, the utilized systems-based quantitative model for inverse/regular wedge cam design coupled with robust sensitivity design optimization automatically develops and locates the perfect cam in connection to the overall mechanism system design layout within context of the desired self-centering function.

Keywords

Self-Centering Wedge Cam Mechanism, Clamping Force Convergence & Stabilization, Robust Design, Robust Design Optimization, Nonlinear

Programming, Concurrent Engineering

1. Introduction

In the development of self-centering devices which clamp around cylindrical workpieces, there are several different existing kinematic design configurations which attempt to embed robustness and various optimization characteristics as well as produce the type of desired functionality in relation to the intended application set forth by the designer. The various practical configurations of such devices usually include anywhere from two to four points of contact. As a related example, self-centering steady rest products/utility patents used for gripping cylindrical workpieces involved in CNC lathe machining processes revolve around three-point contact clamping devices [1]-[19]. Another similar clamping device design includes a patented oil & gas wrench involving similar, but different, three-point contact self-centering motion serving as a method for gripping and positioning thin-walled cylinders [20]. Other comparable clamping device designs include a two-point pipe clamping chuck design in addition to a two-arm holding self-centering pipeline clamping device among others [21] [22].

In connection, and regarding diverse applicability of related gripping mechanisms, Afandiyev and Nuriyev discuss the occurrence of clamping devices being widely used in various industries with constantly increasing needs, especially in relation to processing accuracy and the forces acting on the clamped part. The reliability of such devices in terms of their use on thin-walled cylinders, in particular drill pipes, is highlighted due to plastic deformations being highly prevalent in clamping zones as a result of current clamping devices creating uneven loading arrangements with associated contact pressure distributions/compressive stresses exceeding the pipe material yield strength. In an effort to remedy these issues involving the state of the pipe and holding capacity of the clamping device, a concept of a pipe clamping chuck design with basic design detail is provided [21].

Additionally, Haixia, Liquan, Shiqing, and Xianchao discuss multifunctional pipeline repair machinery being used in the deep-sea arena along with the difficulty of gripping pipelines while ensuring their concentricity between cutter heads and the pipeline during operation. In view of this, a new design involving a two-arm holding self-centering pipeline clamping device is proposed which involves two groups of parallelogram double-rocker and cranking block mechanisms. The recommended design is extensive in presentment with schematic representations along with 3D modeling as well as detailed calculations coupled to CAE simulation along with being accompanied by the real clamping device prototype with satisfactory testing results [22].

Furthermore, Mhamane, Bavadekar, Dhokale, Hogade, Patil, and Survase among others discuss the use of a self-centering steady rest for eliminating problems involving vibration and deflection on workpieces while machining. They also

describe its facilitation regarding an increase in productivity by reducing cycle time along with being able to obtain higher accuracy and good surface finish. Consequently, a regular wedge cam design within the context of a self-centering steady rest is discussed for improving these characteristics with design aspects being presented based on a graphical incremental angle approach within the computer-aided design environment [23]-[25]. Moreover, and expanding on self-centering steady rests and their inherent cam design due to the proposed optimization-based research being centered around similar three-point clamping device design, previous existing related theory explores analytical approaches to the development of the regular wedge cam path involving parametric equation formulation through trigonometric and velocity techniques as well as approximating the cam contour using regression analysis and first-order iterative solver approximation procedures [26]-[35].

As previously discussed, there is an increasing need for reliability involving clamping accuracy, force transmission, vibration minimization, material deformation, productivity, and more. Improving these characteristics is not a trivial exercise due to manufacturing, quality, and engineering considerations whereby the design and analysis variables are rather numerous and complex therefore making it difficult for combining and directing toward optimizing characteristics through typical manual type adjustments in a computer-aided design environment or by analytical presentments that are lacking in robustness from an optimization perspective [36]. Consequently, this can be better achieved through the application of robust design/robust design optimization methods to a recently developed generalized and rigorous systems-based theoretical engineering model toward achieving world-class engineering and design intent [37].

Therefore, the research entailed herein presents an optimization technique based on nonlinear interior point algorithms and/or second derivatives that inherently leads to minimization of clamping force variation in conjunction with force convergence and stabilization effects for designing optimal three-point self-centering mechanisms about a variable workpiece diameter of both the inverse and regular wedge cam types. This is useful for extending the usage of such toward the design and development of devices similar to existing practical application within the manufacturing industry regarding self-centering steady rests in addition to the oil & gas industry involving pipe handling and/or pipeline repair machinery as well as finding its way into other industries such as aerospace, construction equipment, and many other potential industry applications whereby the efficiency and utility of such vigorously engineered and optimized product designs resulting from this applied theoretical optimization model may be beneficial.

Contained within, a theoretical inverse/regular wedge cam theory is utilized in context of a product design concept with a discussion on applying advanced robust design optimization techniques revealing significantly novel results related to improving force convergence and stabilization between grippers across the full diametral surface range for substantiating the usefulness and practical application

of the selected systems-based quantitative model for advancing/developing new and improved devices of the associated diametral self-centering type. Additionally, conclusory commentary related to this research along with potential limitations in conjunction with future research involving computer-aided engineering and feasibility robust design optimization integration in connection with concurrent engineering is reflected upon.

2. Methodology

Regarding the use of a recently developed inverse/regular wedge cam theory [37], the specific generalized robust systems-based quantitative model and associated framework, as shown in **Figure 1**, allows for the application of state-of-the-art robust design optimization techniques for improving product designs to meet the required high-quality demands in alignment with industry needs of today.

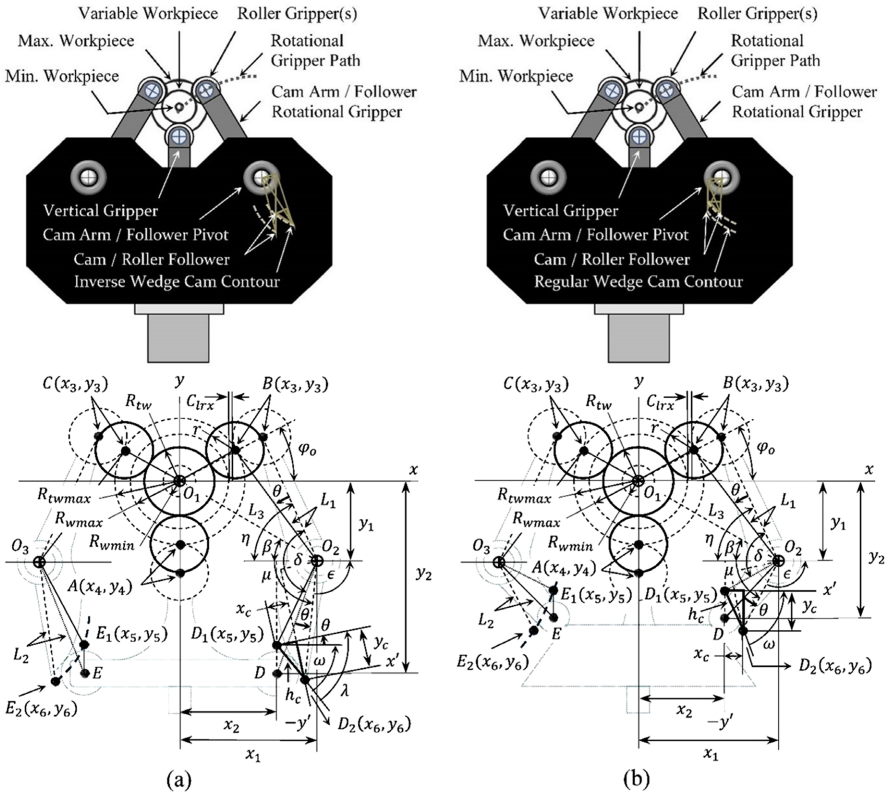

Figure 1. The kinematic self-centering motion layout (a) Inverse wedge cam, (b) Regular wedge cam.

In connection, and as previously discussed, unequal clamping forces around cylindrical workpieces may create issues in terms of contact stresses regarding material deformations related to "pipe crushing" as well as create dynamic issues concerning vibrations among having other related issues in context of variable range self-centering robotic grippers utilized for machining or other pur-

poses. Consequently, and extending the task of robust design optimization to this innovative systems-based framework, characteristics of clamping stability in relation to the equalization of clamping force distributions on the workpiece are first examined through engineering judgment and then through the use of sensitivity analysis involving an objective function and associated constraints while employing interior point algorithms and second derivatives optimization procedures for obtaining an optimal solution in context of the various equations obtained from [37].

As such, several calculated/driven fixed analysis variable equations are provided below where R_{wmax}, r, C_{lrx}, φ_o, x_1, y_1, x_2, and y_2 are specified/driving analysis variables respectively denoted as the maximum actual workpiece radius, gripper roller radius, horizontal clearance, initial contact angle, horizontal and vertical coordinates from points O_1 to O_2, and horizontal and vertical coordinates from points O_1 to D.

$$R_{twmax} = \frac{R_{wmax} + C_{lrx} + r}{\cos\varphi_o} - r \tag{1}$$

$$L_1 = \sqrt{\left(x_1 - \left(R_{twmax} + r\right)\cos\varphi_o\right)^2 + \left(y_1 + \left(R_{twmax} + r\right)\sin\varphi_o\right)^2} \tag{2}$$

$$L_2 = \sqrt{\left(x_2 - x_1\right)^2 + \left(y_2 - y_1\right)^2} \tag{3}$$

$$L_3 = \sqrt{x_1^2 + y_1^2} \tag{4}$$

$$\eta = \frac{\pi}{2} - \tan^{-1}\frac{x_1 - \left(R_{twmax} + r\right)\cos\varphi_o}{y_1 + \left(R_{twmax} + r\right)\sin\varphi_o} \tag{5}$$

$$\beta = \tan^{-1}\frac{y_1}{x_1} \tag{6}$$

Additionally, parametric inverse/regular wedge cam equations based on the transformation method are defined as follows where $y_5(\theta)$ is a variable coordinate point, θ is an independent cam rotation variable, and subscripts i and r are used to distinguish between the inverse and regular cam equation types.

$$\begin{aligned} & y_5(\theta) = y_2 - \left(R_{twmax} - R_{tw}(\theta)\right) \\ & \Rightarrow y_2 - \Bigg(R_{twmax} - \Bigg(-r + \sqrt{\Big(L_3^2 - 2x_1\cos\theta\left(x_1 - \left(r + R_{twmax}\right)\cos\varphi_o\right) \\ & \quad + \left(x_1 - \left(r + R_{twmax}\right)\cos\varphi_o\right)^2 + 2y_1\left(x_1 - \left(r + R_{twmax}\right)\cos\varphi_o\right)\sin\theta \\ & \quad - 2y_1\cos\theta\left(y_1 + \left(r + R_{twmax}\right)\sin\varphi_o\right) - 2x_1\sin\theta\left(y_1 + \left(r + R_{twmax}\right)\sin\varphi_o\right) \\ & \quad + \left(y_1 + \left(r + R_{twmax}\right)\sin\varphi_o\right)^2\Big)\Bigg)\Bigg) \end{aligned} \tag{7}$$

$$x_{c_i}(\theta) = \left(x_2 - x_1\right) - \left(x_2 - x_1\right)\cos\theta + \left(y_5(\theta) - y_1\right)\sin\theta \tag{8}$$

$$y_{c_i}(\theta) = \left(y_2 - y_1\right) - \left(x_2 - x_1\right)\sin\theta - \left(y_5(\theta) - y_1\right)\cos\theta \tag{9}$$

$$x_{c_r}(\theta) = x_1 - x_2 + (x_2 - x_1)\cos\theta + (y_2 - y_1)\sin\theta \tag{10}$$

$$y_{c_r}(\theta) = -(x_2 - x_1)\sin\theta + (y_2 - y_1)\cos\theta - y_5(\theta) \tag{11}$$

Furthermore, the maximum cam rotation equation is defined for establishing the proper termination of cam path point(s).

$$\theta_{max} = \eta - \beta - \cos^{-1}\frac{L_1^2 + L_3^2 - (r + R_{wmin})^2}{2L_1L_3} \tag{12}$$

With having the cam path(s) defined, the associated statics diagram of the self-centering mechanism is provided further below within **Figure 2**. The following related equations include the contact angle φ, the cam path slope m_c, pressure angle ϕ, as well as moment arms L_m and d_m for defining the force equations.

$$\begin{aligned}\varphi(\theta) &= \tan^{-1}\frac{y_3(\theta)}{x_3(\theta)} \\ &= \tan^{-1}\frac{-y_1 - (x_1 - (R_{twmax} + r)\cos\varphi_o)\sin\theta + (y_1 + (R_{twmax} + r)\sin\varphi_o)\cos\theta}{x_1 - (x_1 - (R_{twmax} + r)\cos\varphi_o)\cos\theta - (y_1 + (R_{twmax} + r)\sin\varphi_o)\sin\theta}\end{aligned} \tag{13}$$

$$\alpha(\theta) = \eta - \beta - \theta \tag{14}$$

$$\psi(\theta) = \pi - (\varphi(\theta) + \beta + \alpha(\theta)) \tag{15}$$

$$m_c(x_c) = \frac{\mathrm{d}y_c(x_c)}{\mathrm{d}x_c} \Rightarrow \frac{\mathrm{d}y_c(\theta(x_c))}{\mathrm{d}\theta(x_c)} \div \frac{\mathrm{d}x_c(\theta(x_c))}{\mathrm{d}\theta(x_c)} \tag{16}$$

$$\rho_i(\theta) = \left|\tan^{-1} m_c(\theta)\right| - \theta \tag{17}$$

$$\rho_r(\theta) = \left|\tan^{-1} m_c(\theta)\right| \tag{18}$$

$$\Omega(\theta) = \frac{\pi}{2} - \rho(\theta) \tag{19}$$

$$\phi_i(\theta) = \left|\Omega(\theta) - \tan^{-1}\frac{x_5 - x_1}{y_5(\theta) - y_1}\right| \tag{20}$$

$$\begin{aligned}\phi_r(\theta) &= \left|\Omega(\theta) - \tan^{-1}\frac{x_6(\theta) - x_1}{y_6(\theta) - y_1}\right| \\ &= \left|\Omega(\theta) - \tan^{-1}\frac{x_1 + (x_2 - x_1)\cos\theta + (y_2 - y_1)\sin\theta - x_1}{y_1 - (x_2 - x_1)\sin\theta + (y_2 - y_1)\cos\theta - y_1}\right|\end{aligned} \tag{21}$$

$$L_{mi}(\theta) = \sqrt{(x_1 - x_5)^2 + (y_5(\theta) - y_1)^2} \tag{22}$$

$$L_{mr}(\theta) = L_2 \tag{23}$$

$$d_m(\theta) = \frac{L_m(\theta)\cos\phi(\theta)}{\sin\Omega(\theta)} + y_1(\theta)\cot\Omega(\theta) + x_1 \tag{24}$$

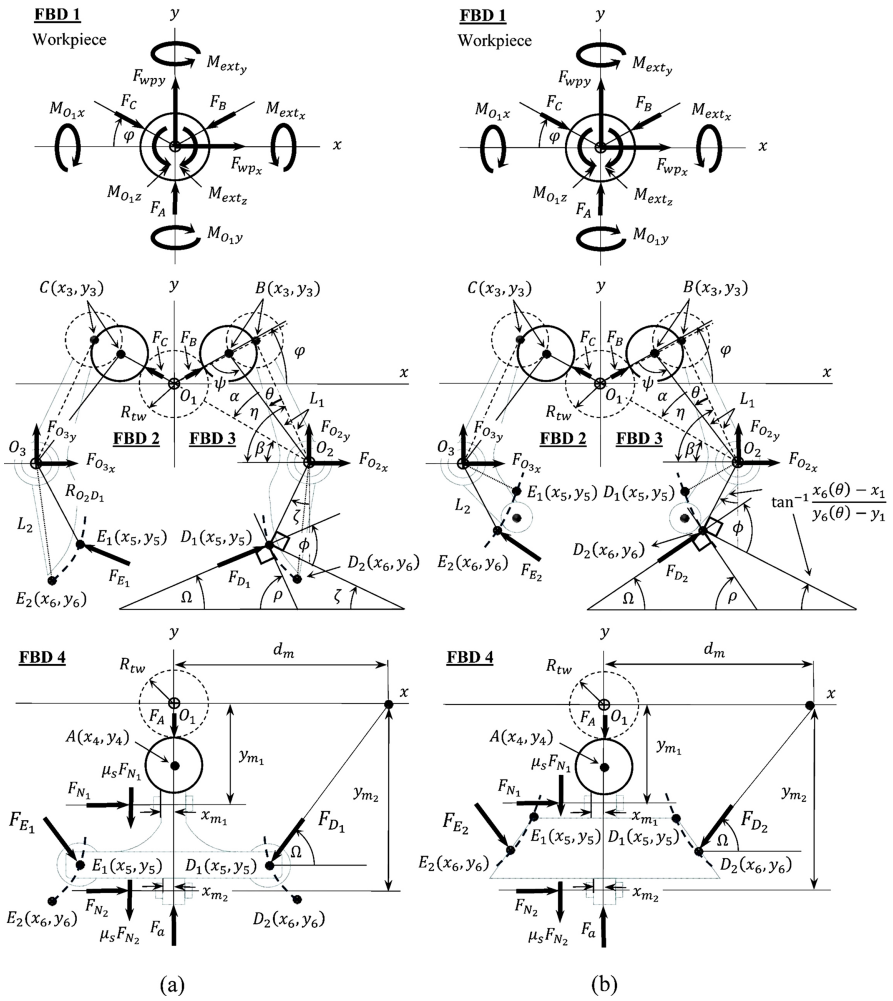

Figure 2. Free-body diagrams for force transmission. (a) Inverse wedge cam, (b) Regular wedge cam.

Prior to defining the force equations, the spatial derivatives of the inverse/regular cam path(s) and associated equations that determine the cam path slope(s) are defined as:

$$a_{1_i}(\theta) = y_4(\theta) + y_2 - y_1 - R_{twmax} - r \tag{25}$$

$$b_{1_i} = x_2 - x_1 \tag{26}$$

$$a_{2_i} = 2y_1\left(x_1 - \left(R_{twmax} + r\right)\cos\varphi_o\right) \tag{27}$$

$$b_{2_i} = 2x_1\left(x_1 - \left(R_{twmax} + r\right)\cos\varphi_o\right) \tag{28}$$

$$a_{1_r} = 2y_1\left(x_1 - \left(R_{twmax} + r\right)\cos\varphi_o\right) \tag{29}$$

$$b_{1_r} = 2x_1\left(x_1 - \left(R_{twmax} + r\right)\cos\varphi_o\right) \tag{30}$$

$$a_{2_r} = -2x_1\left(y_1 + \left(R_{twmax} + r\right)\sin\varphi_o\right) \tag{31}$$

$$b_{2_r} = 2y_1\left(y_1 + R_{twmax} + r\right)\sin\varphi_o\right) \tag{32}$$

$$c_{w_{1_i}}(\theta) = a_{1_i}(\theta)\cos\theta + b_{1_i}\sin\theta \tag{33}$$

$$c_{w_{2_i}} = a_{2_i}\cos\theta + b_{2_i}\sin\theta \tag{34}$$

$$c_{w_{6_i}}(\theta) = -b_{1_i}\cos\theta + a_{1_i}(\theta)\sin\theta \tag{35}$$

$$c_{w_{1_r}}(\theta) = a_{1_r}\cos\theta + b_{1_r}\sin\theta \tag{36}$$

$$c_{w_{2_r}} = a_{2_r}\cos\theta + b_{2_r}\sin\theta \tag{37}$$

$$\frac{\mathrm{d}x_{c_i}(\theta)}{\mathrm{d}\theta} = c_{w_{1_i}}(\theta) + \frac{\left(c_{w_{2i}} + c_{w_{3_i}}\right)\sin\theta}{2y_4(\theta)} \tag{38}$$

$$\frac{\mathrm{d}y_{c_i}(\theta)}{\mathrm{d}\theta} = c_{w_{6i}}(\theta) - \frac{\left(c_{w_{2i}} + c_{w_{3_i}}\right)\cos\theta}{2y_4(\theta)} \tag{39}$$

$$\frac{\mathrm{d}x_{c_r}(\theta)}{\mathrm{d}\theta} = (y_2 - y_1)\cos\theta - (x_2 - x_1)\sin\theta \tag{40}$$

$$\frac{\mathrm{d}y_{c_r}(\theta)}{\mathrm{d}\theta} = -(x_2 - x_1)\cos\theta - (y_2 - y_1)\sin\theta - \frac{c_{w_{1_r}}(\theta) + c_{w_{2r}}}{2y_4(\theta)} \tag{41}$$

The translational and rotational gripper forces are given below in sequence where forces F_{wpx} and F_{wpy} are external reaction forces along the workpiece axes. Further information regarding the determination of these reaction forces is provided within [37].

$$\begin{aligned} F_A(\theta) = {} & \frac{1}{L_m(\theta)\cos\phi(\theta)\sin\varphi(\theta) + L_1\sin\psi(\theta)\sin\Omega(\theta)} \\ & \times\Big(F_a L_m(\theta)\cos\phi(\theta)\sin\varphi(\theta) \\ & - L_1\sin\psi(\theta)\Big(F_{wp_y}\sin\Omega(\theta) + F_{wp_x}\mu_s\cos\Omega(\theta)\tan\varphi(\theta)\Big)\Big) \end{aligned} \tag{42}$$

$$\begin{aligned} F_B(\theta) = {} & \frac{1}{2\left(L_m(\theta)\cos\phi(\theta)\sin\varphi(\theta) + L_1\sin\psi(\theta)\sin\Omega(\theta)\right)} \\ & \times\Big(L_m(\theta)\cos\phi(\theta)\Big(F_a + F_{wp_y} + F_{wp_x}\tan\varphi(\theta)\Big) \\ & + F_{wp_x}L_1\sec\varphi(\theta)\sin\psi(\theta)\big(\sin\Omega(\theta) - \mu_s\cos\Omega(\theta)\big)\Big) \end{aligned} \tag{43}$$

Moving further, and corresponding to exercising engineering judgment regarding three-point self-centering diametral surface contact, it is beneficial for the angles between each contact force to be equal at 120˚ apart from each other. Accordingly, the initial contact angle φ_o from the horizon is defined at 30˚. This aids in reducing design variables and associated variation as part of applying robust design intent prior to incorporating more advanced design optimization techniques.

In connection, and regarding a symmetrical loading assumption, sensitivity robustness is then invoked for reducing further variation between contact forces and across the entire design range. For accomplishing this, minimization of a suitable proxy as per the standard deviation of the force differences be-

tween F_A and F_B over the full cam rotation design range occurs through the following equation, where index n is the specified number of clamping force differences with the angle increment of cam rotation being $\theta_i = \theta_{max}/n$.

$$v(\theta) = F_B(\theta) - F_A(\theta) \tag{44}$$

$$\sigma_{STD}(n) = \sqrt{\frac{1}{n-1}\left(\sum_{n=1}^{n} v^2(n\theta_i) + \frac{1}{n}\left(\sum_{n=1}^{n} v(n\theta_i)\right)^2\right)} \tag{45}$$

In conjunction with the objective function provided regarding the minimization of Equation 45, design space and clamping force range constraints are imposed on the optimization problem and corresponding example designs.

For limiting the lower and upper clamping force boundaries in accordance with suitable clamping force fluctuations within the prescribed design range, various constraints are presented through the following equations. To note, the specific equations regarding clamping force range constraints cannot be completely generalized and may need to be modified to specified design requirements using practical engineering judgment.

$$1 \le \frac{\max F_A(\theta)}{\min F_A(\theta)} \le 2 \tag{46}$$

$$\frac{F_a}{4} \le F_A(0) \tag{47}$$

$$\frac{F_a}{4} \le F_B(0) \tag{48}$$

$$\frac{F_a}{4} \le \min F_A(\theta) \le \frac{F_a}{2} \tag{49}$$

$$\frac{F_a}{4} \le \max F_A(\theta) \le \frac{F_a}{2} \tag{50}$$

$$\frac{F_a}{4} \le \min F_B(\theta) \le \frac{F_a}{2} \tag{51}$$

$$\frac{F_a}{4} \le \max F_B(\theta) \le \frac{F_a}{2} \tag{52}$$

Prior to the presentment of various example designs and associated optimization results, the following analysis equations are defined for determining average force convergence effects f_{cavg} as well as average slope proxies, m_A and m_B, with associated average clamping force flattening effects f_{favg} for use in conjunction with optimization results. Additionally, the standard deviation/maximum force variance improvement ratio $\sigma_{STD\ IMPRV}$ is presented for examining the results achieved through utilization of the design optimization procedure as previously provided. To note, subscripts o and f appearing within the following equations indicate before (original) and after (final) optimization respectively.

$$f_{c_{avg}} = \frac{1}{2}\left(\frac{\left(\max F_A(\theta) - \min F_A(\theta)\right)_o}{\left(\max F_A(\theta) - \min F_A(\theta)\right)_f} + \frac{\left(\max F_B(\theta) - \min F_B(\theta)\right)_o}{\left(\max F_B(\theta) - \min F_B(\theta)\right)_f} \right) \tag{53}$$

$$m_A = \frac{\max F_A(\theta) - \min F_A(\theta)}{\theta_{max}} \tag{54}$$

$$m_B = \frac{\max F_B(\theta) - \min F_B(\theta)}{\theta_{max}} \tag{55}$$

$$f_{f_{avg}} = \frac{1}{2}\left(\frac{m_{A_o}}{m_{A_f}} + \frac{m_{B_o}}{m_{B_f}} \right) \tag{56}$$

$$\sigma_{STD\ IMPRV} = \frac{\sigma_{STDo}(n)}{\sigma_{STD\,f}(n)} \tag{57}$$

3. Results with Results Discussion

For demonstrating the novelty in having a systems-based framework in combination with advanced design optimization, three (before optimization) self-centering inverse and regular wedge cam designs as per Table 1 below are constructed from the theoretical models developed in accordance with [37] in preparation for performing sensitivity robust design optimization.

Table 1. Specified analysis variables for use when optimizing the self-centering inverse and regular wedge cam designs.

Variables	Example 1	Example 2	Example 3
R_{wmax}	4.0000 in. (0.1016 m)	4.0000 in. (0.1016 m)	4.0000 in. (0.1016 m)
R_{wmin}	0.5000 in. (0.0127 m)	1.5000 in. (0.0381 m)	2.0000 in. (0.0506 m)
r	2.5000 in. (0.0635 m)	2.0000 in. (0.0506 m)	2.0000 in. (0.0506 m)
C_{lrx}	0.1250 in. (0.0032 m)	0.5000 in. (0.0127 m)	0.2500 in. (0.0064 m)
φ_o	14.07 deg (0.2456 rad)	30.00 deg (0.5236 rad)	30.00 deg (0.5236 rad)
x_1	4.6875 in. (0.1191 m)	4.6875 in. (0.1191 m)	4.6875 in. (0.1191 m)
y_1	7.6898 in. (0.1953 m)	8.3656 in. (0.2125 m)	8.0769 in. (0.2052 m)
x_2	6.6250 in. (0.1683 m)	6.5000 in. (0.1651 m)	6.2500 in. (0.1588 m)
y_2	13.2798 in. (0.3373 m)	13.9556 in. (0.3545 m)	13.6669 in. (0.3471 m)
x_{cg}	1 in. (0.0127 m)	1 in. (0.0127 m)	1 in. (0.0127 m)
y_{cg}	1 in. (0.0127 m)	1 in. (0.0127 m)	1 in. (0.0127 m)
F_a	1000 lb. (4.448 kN)	1000 lb. (4.448 kN)	1000 lb. (4.448 kN)
F_{wp_x}	0 lb. (0 kN)	0 lb. (0 kN)	0 lb. (0 kN)
F_{wp_y}	0 lb. (0 kN)	0 lb. (0 kN)	0 lb. (0 kN)

Furthermore, and with using the Wolfram Mathematica FindMinimum function which implements numerical local optimization relying on nonlinear interior point algorithms and/or second derivatives due to nonlinearities involved within the example designs, the associated clamping force graphs pertaining to before and after optimization with related aspects regarding force convergence and stabilization effects (over the entire cam rotation range) among others are shown within Figure 3 below.

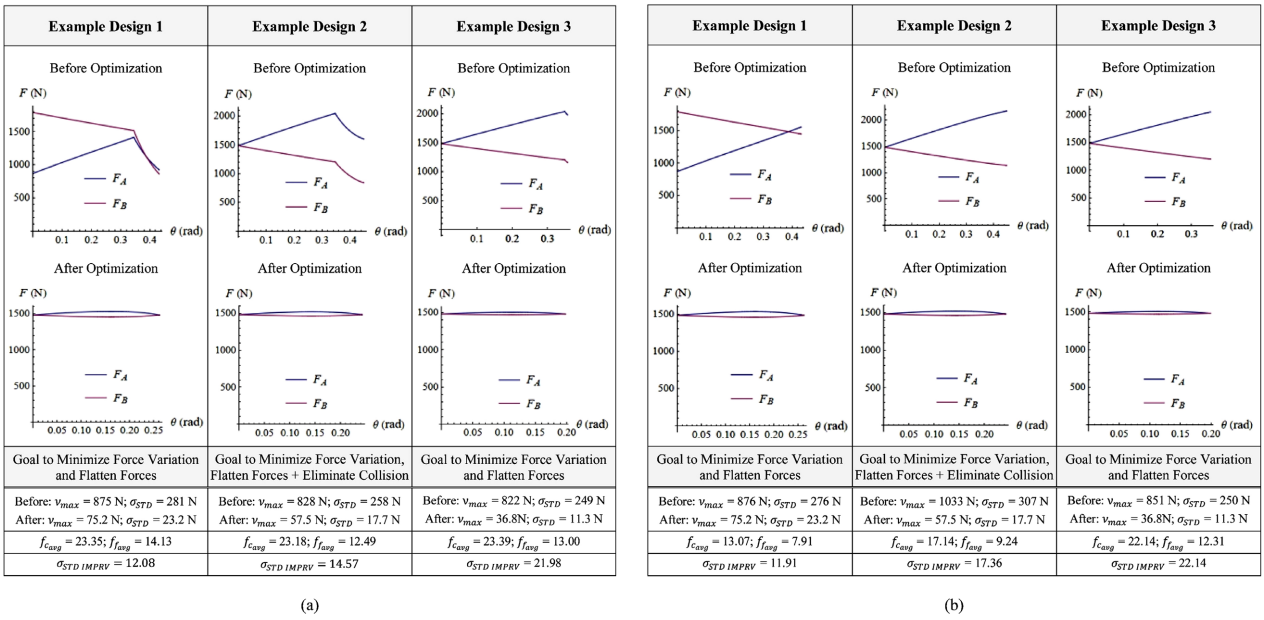

Figure 3. Before and after optimization clamping force graphs and associated results. (a) Inverse wedge cam, (b) Regular wedge cam.

While it is a known challenge to design three-point diametral self-centering devices with the function of maintaining the same force amount between grippers over the entire gripping range, strong positive changes in force variance reduction and flattening effects (on the order of an average of approximately 15 and 10 times respectively) ensue across all design cases for both inverse and regular wedge cam types. The presented contribution is highlighted due to this problem typically requiring an operator or some other method of modifying the actuator's input pressure as the gripper moves throughout the range of workpiece diameters (or cam rotation range), which is inefficient, leaves room for operator error, and can potentially cause workpiece damage thereby leading to possible safety issues.

For further discussion of results while emphasizing the third inverse/regular design case(s), it is seen in Figure 3—Example Design 3 that gripper forces start at about 1500 N and diverge to about 1200 N and 2050 N respectively ($v_{max,o}$ = 850 N) for the original design case, which poses an engineering issue. Moreover, and after optimization, gripper forces start and end at about 1500 N with very little divergence ($v_{max,f}$ = 37 N) over the full cam rotation range, which will generally be negligible from an engineering application context.

Consequently, and as substantiated herein, the derived generalized systems-based quantitative model coupled with sensitivity robust design optimization automatically develops and locates the perfect cam and overall mechanism system design layout within context of the desired self-centering function.

To validate the design optimization results shown in **Figure 3**, computer-aided force simulations pertaining to regular wedge cam designs (before and after optimization) are performed for comparing against theoretically obtained results. For accomplishing this, and due to simulation difficulties occurring with the use of an activation force of F_a = 1000 lb. (4448 N), the following CAE simulation figures are constructed based on an activation force of F_a = 100 lb. (445 N) with the numerical simulation results being scaled by a multiple of 10 via force similitude analysis to match the value used for prior theoretical optimization results. The before and after optimization results are shown in **Figures 4~17** below.

Regular Wedge Cam Design Concept at Various Angle Increments (Before Optimization)

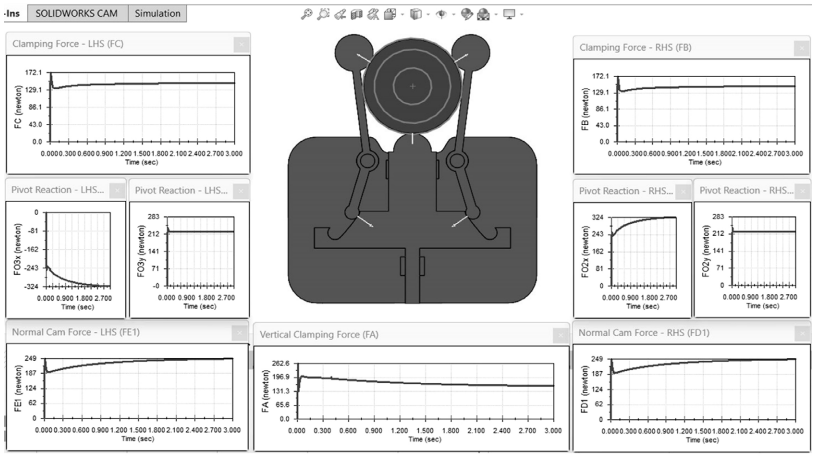

(N)	Given	Max. Error
F_a	4448 @ Actuator (z = 0 m)	4.82%
F_{wp_x}	0 Along WP (z = 1.37 m)	Avg. Error
F_{wp_y}	0 (z = 0.914 m); 0 (z = 1.37 m)	2.43%
(N)	Simulated	Theory	Error %
F_A	1554	1483	4.82
F_B	1456	1482	1.77
F_C	1456	1482	1.77
F_{D_2}	2467	2540	2.87
F_{E_2}	2467	2540	2.87
F_{O_2x}	3239	3347	3.22
F_{O_2y}	2210	2224	0.65
F_{O_3x}	3239	3347	3.22
F_{O_3y}	2210	2224	0.65

Figure 4. Computer-aided symmetrical force simulation for regular wedge cam example 3 before optimization at $\theta = 0^\circ$.

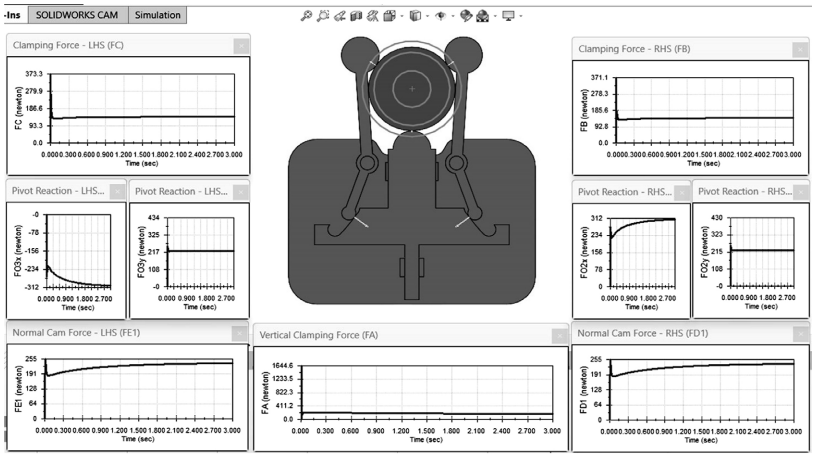

(N)	Given	Max. Error
F_a	4448 @ Actuator (z = 0 m)	2.30%
F_{wp_x}	0 Along WP (z = 1.37 m)	Avg. Error
F_{wp_y}	0 (z = 0.914 m); 0 (z = 1.37 m)	1.20%
(N)	Simulated	Theory	Error %
F_A	1637	1600	2.30
F_B	1412	1424	0.84
F_C	1412	1424	0.84
F_{D_2}	2357	2389	1.36
F_{E_2}	2357	2389	1.36
F_{O_2x}	3051	3097	1.46
F_{O_2y}	2211	2224	0.59
F_{O_3x}	3051	3097	1.46
F_{O_3y}	2211	2224	0.59

Figure 5. Computer-aided symmetrical force simulation for regular wedge cam example 3 before optimization at $\theta = 4^\circ$.

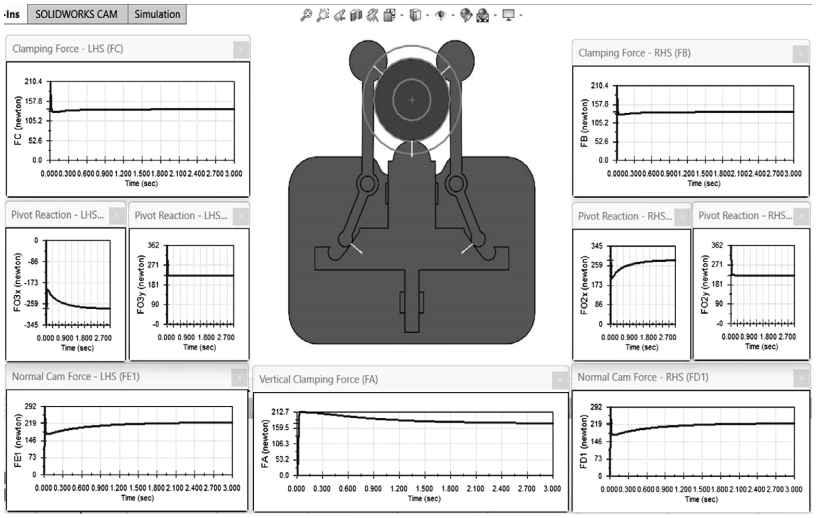

(N)	Given	Max. Error
F_a	4448 @ Actuator (z = 0 m)	1.47%
F_{wp_x}	0 Along WP (z = 1.37 m)	Avg. Error
F_{wp_y}	0 (z = 0.914 m); 0 (z = 1.37 m)	0.87%
(N)	Simulated	Theory	Error %
F_A	1740	1714	1.47
F_B	1358	1367	0.64
F_C	1358	1367	0.64
F_{D_2}	2218	2240	0.96
F_{E_2}	2218	2240	0.96
F_{O_2x}	2810	2839	1.06
F_{O_2y}	2212	2224	0.52
F_{O_3x}	2810	2839	1.06
F_{O_3y}	2212	2224	0.52

Figure 6. Computer-aided symmetrical force simulation for regular wedge cam example 3 before optimization at $\theta = 8^\circ$.

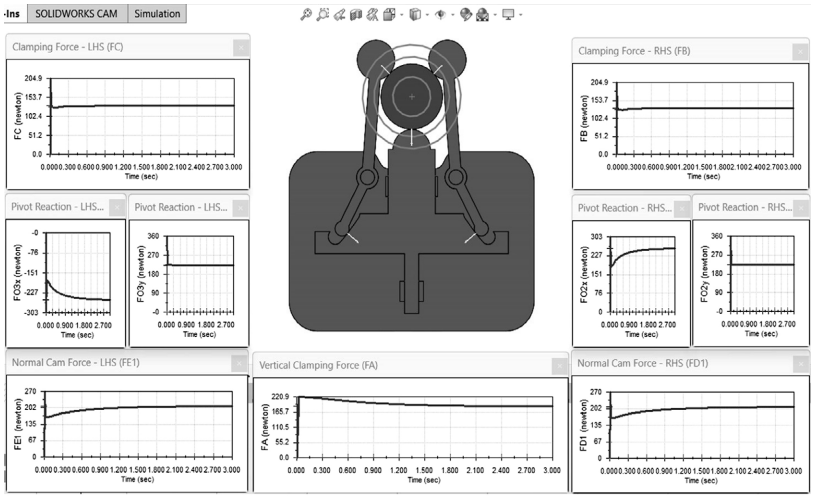

(N)	Given	Max. Error
F_a	4448 @ Actuator (z = 0 m)	0.93%
F_{wp_x}	0 Along WP (z = 1.37 m)	Avg. Error
F_{wp_y}	0 (z = 0.914 m); 0 (z = 1.37 m)	0.64%
(N)	Simulated	Theory	Error %
F_A	1844	1827	0.93
F_B	1304	1311	0.50
F_C	1304	1311	0.50
F_{D_1}	2072	2086	0.68
F_{E_1}	2072	2086	0.68
F_{O_2x}	2544	2563	0.76
F_{O_2y}	2214	2224	0.45
F_{O_3x}	2544	2563	0.76
F_{O_3y}	2214	2224	0.45

Figure 7. Computer-aided symmetrical force simulation for regular wedge cam example 3 before optimization at $\theta = 12^\circ$.

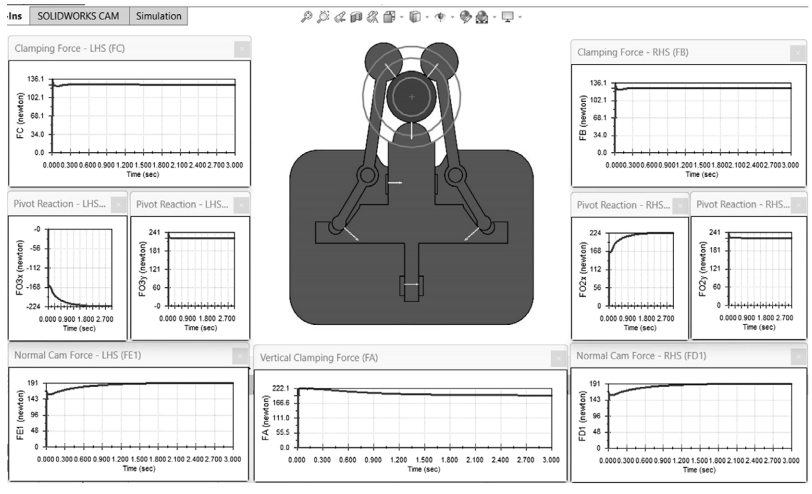

(N)	Given	Max. Error
F_a	4448 @ Actuator (z = 0 m)	0.58%
F_{wp_x}	0 Along WP (z = 1.37 m)	Avg. Error
F_{wp_y}	0 (z = 0.914 m); 0 (z = 1.37 m)	0.48%
(N)	Simulated	Theory	Error %
F_A	1947	1936	0.57
F_B	1251	1256	0.42
F_C	1251	1256	0.42
F_{D_2}	1912	1921	0.50
F_{E_2}	1912	1921	0.50
F_{O_2x}	2241	2254	0.58
F_{O_2y}	2216	2224	0.38
F_{O_3x}	2241	2254	0.58
F_{O_3y}	2216	2224	0.38

Figure 8. Computer-aided symmetrical force simulation for regular wedge cam example 3 before optimization at $\theta = 16^\circ$.

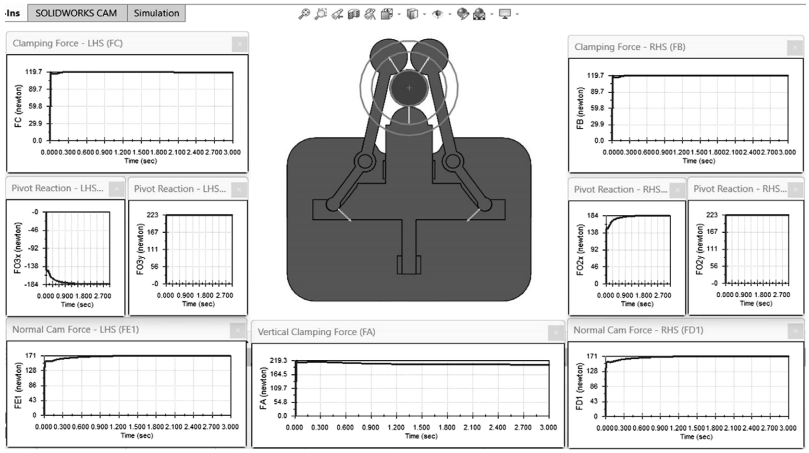

(N)	Given	Max. Error
F_a	4448 @ Actuator (z = 0 m)	2.56%
F_{wp_x}	0 Along WP (z = 1.37 m)	Avg. Error
F_{wp_y}	0 (z = 0.914 m); 0 (z = 1.37 m)	1.34%
(N)	Simulated	Theory	Error %
F_A	2022	2040	0.88
F_B	1185	1204	1.57
F_C	1185	1204	1.57
F_{D_2}	1713	1733	1.17
F_{E_2}	1713	1733	1.17
F_{O_2x}	1839	1887	2.56
F_{O_2y}	2218	2224	0.30
F_{O_3x}	1839	1887	2.56
F_{O_3y}	2218	2224	0.30

Figure 9. Computer-aided symmetrical force simulation for regular wedge cam example 3 before optimization at $\theta = 20^\circ$.

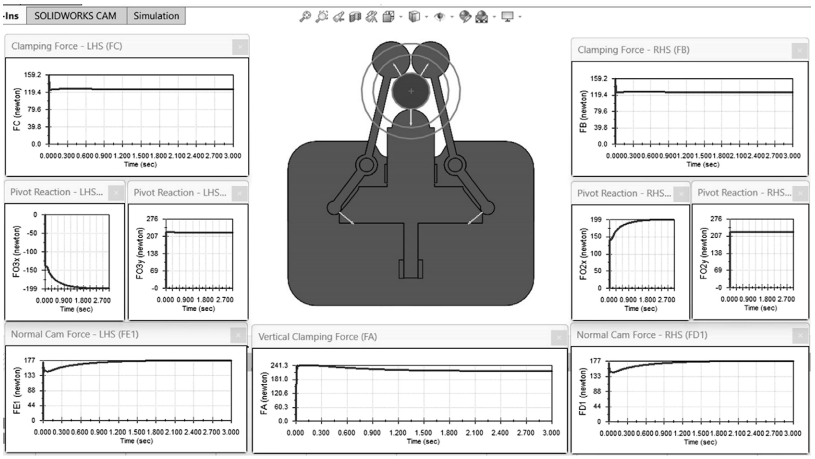

(N)	Given	Max. Error
F_a	4448 @ Actuator (z = 0 m)	8.14%
F_{wp_x}	0 Along WP (z = 1.37 m)	Avg. Error
F_{wp_y}	0 (z = 0.914 m); 0 (z = 1.37 m)	4.17%
(N)	Simulated	Theory	Error %
F_A	2158	2050	5.28
F_B	1252	1199	4.38
F_C	1252	1199	4.38
F_{D_2}	1768	1712	3.24
F_{E_2}	1768	1712	3.24
F_{O_2x}	1994	1844	8.14
F_{O_2y}	2216	2224	0.37
F_{O_3x}	1994	1844	8.14
F_{O_3y}	2216	2224	0.37

Figure 10. Computer-aided symmetrical force simulation for regular wedge cam example 3 before optimization at $\theta = \theta_{max} = 20.42^\circ$.

(After Optimization)

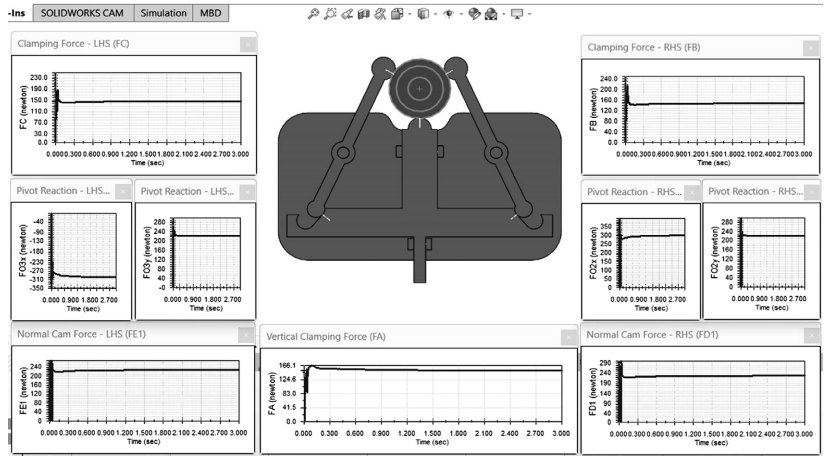

(N)	Given	Max. Error
F_a	4448 @ Actuator (z = 0 m)	1.22%
F_{wp_x}	0 Along WP (z = 1.37 m)	Avg. Error
F_{wp_y}	0 (z = 0.914 m); 0 (z = 1.37 m)	0.78%
(N)	Simulated	Theory	Error %
F_A	1501	1483	1.22
F_B	1469	1483	0.91
F_C	1470	1483	0.84
F_{D_2}	2268	2284	0.67
F_{E_2}	2270	2284	0.61
F_{O_2x}	2995	3021	0.84
F_{O_2y}	2210	2224	0.63
F_{O_3x}	2998	3021	0.77
F_{O_3y}	2212	2224	0.55

Figure 11. Computer-aided symmetrical force simulation for regular wedge cam example 3 after optimization at $\theta = 0^\circ$.

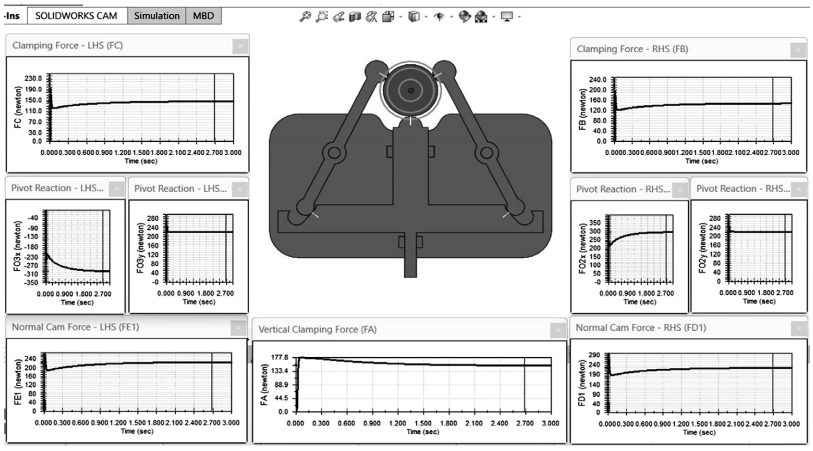

(N)	Given	Max. Error
F_a	4448 @ Actuator (z = 0 m)	1.00%
F_{wp_x}	0 Along WP (z = 1.37 m)	Avg. Error
F_{wp_y}	0 (z = 0.914 m); 0 (z = 1.37 m)	0.72%
(N)	Simulated	Theory	Error %
F_A	1510	1495	1.00
F_B	1463	1477	0.92
F_C	1463	1477	0.92
F_{D_2}	2250	2262	0.54
F_{E_2}	2250	2262	0.54
F_{O_2x}	2963	2988	0.80
F_{O_2y}	2213	2224	0.49
F_{O_3x}	1963	2988	0.80
F_{O_3y}	2213	2224	0.49

Figure 12. Computer-aided symmetrical force simulation for regular wedge cam example 3 after optimization at $\theta = 2^\circ$.

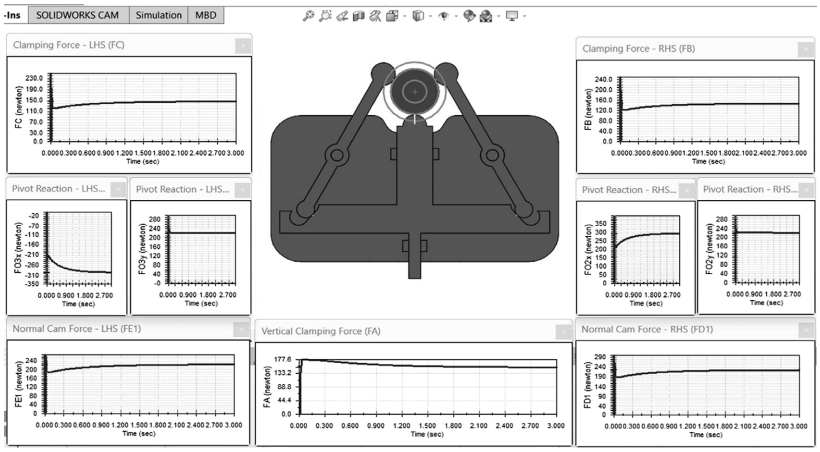

(N)	Given	Max. Error
F_a	4448 @ Actuator (z = 0 m)	0.78%
F_{wp_x}	0 Along WP (z = 1.37 m)	Avg. Error
F_{wp_y}	0 (z = 0.914 m); 0 (z = 1.37 m)	0.58%
(N)	Simulated	Theory	Error %
F_A	1514	1503	0.74
F_B	1461	1473	0.78
F_C	1461	1473	0.78
F_{D_2}	2235	2244	0.42
F_{E_2}	2235	2244	0.42
F_{O_2x}	2941	2960	0..66
F_{O_2y}	2216	2224	0.37
F_{O_3x}	2941	2960	0.66
F_{O_3y}	2216	2224	0.37

Figure 13. Computer-aided symmetrical force simulation for regular wedge cam example 3 after optimization at $\theta = 4^\circ$.

In reviewing **Figures 4~17**, there is only about a 2.5% maximum error across the entire cam rotation range test points for the before optimization CAE simulation results (except for at the end points), and there is

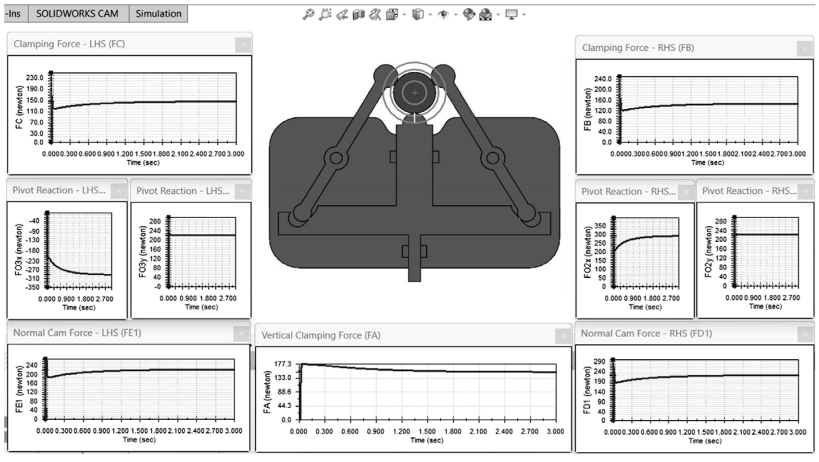

(N)	Given	Max. Error
F_a	4448 @ Actuator (z = 0 m)	0.65%
F_{wp_x}	0 Along WP (z = 1.37 m)	Avg. Error
F_{wp_y}	0 (z = 0.914 m); 0 (z = 1.37 m)	0.44%
(N)	Simulated	Theory	Error %
F_A	1514	1507	0.51
F_B	1461	1471	0.65
F_C	1461	1471	0.65
F_{D_2}	2223	2230	0.30
F_{E_2}	2223	2230	0.30
F_{O_2x}	2923	2939	0.54
F_{O_2y}	2218	2224	0.25
F_{O_3x}	2923	2939	0.54
F_{O_3y}	2218	2224	0.25

Figure 14. Computer-aided symmetrical force simulation for regular wedge cam example 3 after optimization at $\theta = 6^\circ$.

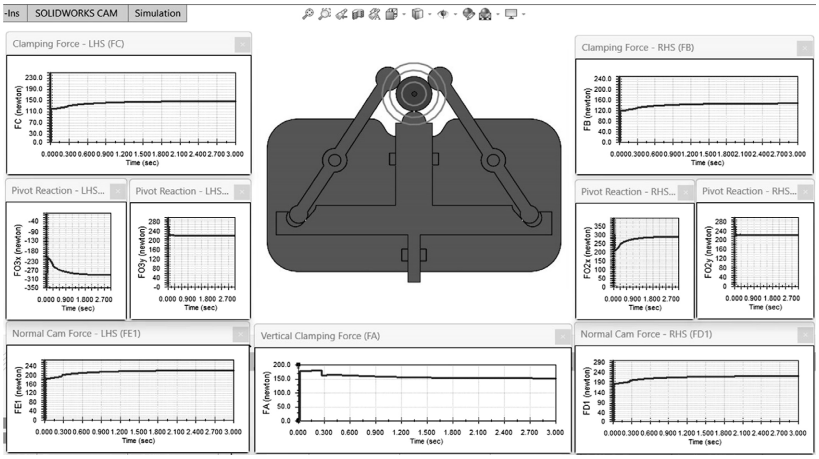

(N)	Given	Max. Error
F_a	4448 @ Actuator (z = 0 m)	0.51%
F_{wp_x}	0 Along WP (z = 1.37 m)	Avg. Error
F_{wp_y}	0 (z = 0.914 m); 0 (z = 1.37 m)	0.31%
(N)	Simulated	Theory	Error %
F_A	1510	1505	0.28
F_B	1464	1471	0.51
F_C	1464	1471	0.51
F_{D_2}	2215	2219	0.18
F_{E_2}	2215	2219	0.18
F_{O_2x}	2914	2925	0.40
F_{O_2y}	2221	2224	0.15
F_{O_3x}	2914	2925	0.40
F_{O_3y}	2221	2224	0.15

Figure 15. Computer-aided symmetrical force simulation for regular wedge cam example 3 after optimization at $\theta = 8^\circ$.

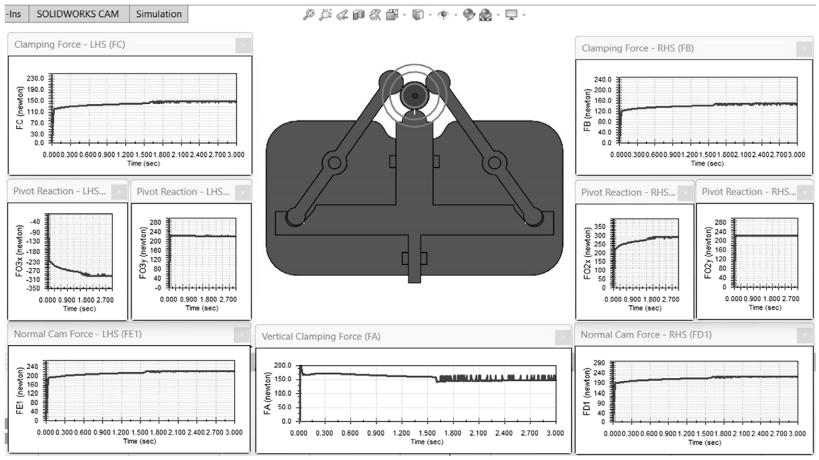

(N)	Given	Max. Error
F_a	4448 @ Actuator (z = 0 m)	3.13%
F_{wp_x}	0 Along WP (z = 1.37 m)	Avg. Error
F_{wp_y}	0 (z = 0.914 m); 0 (z = 1.37 m)	0.77%
(N)	Simulated	Theory	Error %
F_A	1450	1496	3.13
F_B	1484	1476	0.54
F_C	1484	1476	0.54
F_{D_2}	2227	2213	0.60
F_{E_2}	2227	2213	0.60
F_{O_2x}	2942	2923	0.69
F_{O_2y}	2223	2224	0.06
F_{O_3x}	2942	2923	0.69
F_{O_3y}	2223	2224	0.06

Figure 16. Computer-aided symmetrical force simulation for regular wedge cam example 3 after optimization at $\theta = 10^\circ$.

only about a 1% maximum error across the entire cam rotation range test points for the after optimization results (other than when getting close to the very end of the range). The error for all points across the entire workpiece range

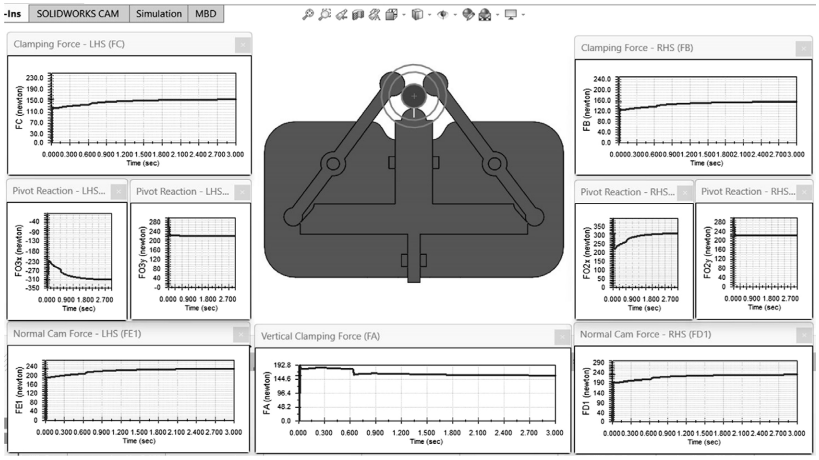

(N)	Given	Max. Error
F_a	4448 @ Actuator (z = 0 m)	6.65%
F_{wp_x}	0 Along WP (z = 1.37 m)	Avg. Error
F_{wp_y}	0 (z = 0.914 m); 0 (z = 1.37 m)	3.86%
(N)	Simulated	Theory	Error %
F_A	1561	1483	5.29
F_B	1543	1483	4.07
F_C	1543	1483	4.07
F_{D_2}	2298	2213	3.86
F_{E_2}	2298	2213	3.86
F_{O_2x}	3121	2926	6.65
F_{O_2y}	2221	2224	0.15
F_{O_3x}	3121	2926	6.65
F_{O_3y}	3221	2224	0.15

Figure 17. Computer-aided symmetrical force simulation for regular wedge cam example 3 after optimization at $\theta = \theta_{max} = 11.35^\circ$.

is reasonable and very low when dealing with mathematical approximation methods utilized within the CAE simulation engine in connection with various tuning parameters.

Concisely summarizing Figures 4~17 into Figure 18 below, both before and after optimization CAE simulation results are shown to be extremely close in accuracy to the theoretical results across the entire cam rotation range thereby validating the theoretical robust design optimization results shown earlier within Figure 3.

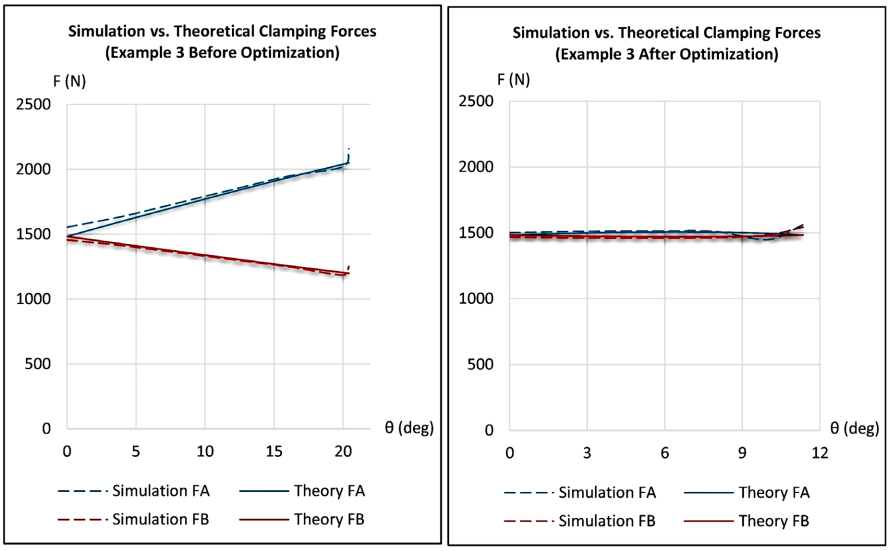

(a) (b)

Figure 18. Simulation vs. Theoretical clamping forces for example 3 (a) Before optimization, (b) After optimization.

4. Conclusions with Limitations

In conclusion, it was found that computer-based design optimization and the associated optimization algorithms are quite powerful with being able to converge to desired optimum designs for assisting the designer in quantitative design synthesis in context of sensitivity robust design optimization. For the associated self-centering cam, good engineering judgement coupled to the systems-based theoretical framework assisted with preliminary robust design efforts regarding a reduction in the complexity of the model and associated variation prior to utilizing more advanced robust design optimization analyses. In connection, variation was further reduced from a physical design perspective for creating better force range convergence and stabilization by employing interior point algorithms and/or second derivatives as per robust design optimization techniques to the finalized systems design model. In all design cases, and due in part to the incorporation of the recently developed robust generalized systems-based wedge cam theory, robustness was seamlessly achieved without complications thereby demonstrating significantly novel results within context of the prescribed design goals. Consequently, the design examples presented

herein illustrate—the power of having a robust systems-based quantitative framework in conjunction with the application of robust design optimization procedures.

However, it is important to emphasize potential limitations of the results. To briefly mention, transmitted variation in concert with the aforementioned optimization methods should incorporate nonnormal input distributions, correlated variables, and some other forms of uncertainty. Additionally, the reliance on specific computational tools and algorithms may limit the general applicability of the findings across different settings or software environments. Furthermore, these methods may lack a concurrent engineering approach which integrates design with manufacturing and inspection. Worth considering, engineering designs represent a compromise among conflicting objectives and sometimes qualitative aspects will drive a design in important ways. In connection, it is just as important to select the best concept for achieving the desired goal as optimization algorithms do not choose a design concept and only help optimize a particular concept. Consequently, the utilization of associated mathematical theories in conjunction with a systems-based concurrent engineering approach should be considered for ensuring a design approaches the best design in relation to achieving true "robustness" as it incorporates a holistic approach to solving engineering problems.

Lastly, while real-world product development activities were outside of the scope and focus of this research manuscript, physical prototypes with experimental testing are crucial for confirming the computer-aided simulations presented herein thereby demonstrating the effectiveness and robustness of a proposed design in a real-world setting including operating conditions, manufacturing tolerances, material properties, and external disturbances. From a pertinent business viewpoint, commercialization of such technologies arising from this research can provide a competitive advantage to organizations and/or serve a useful requirement to society due to the inherent higher quality and functionality that is embedded directly into product designs resulting from the associated combined systems-based theoretical framework and robust design optimization application components during the engineering and design process.

5. Future Research

Before expanding upon future research, it is important to emphasize that robust design/robust design optimization methods are quite mature in terms of research and reasonable practical industry application. Computer-Aided Design & Engineering (CAD/CAE) packages are now offering optimization software as add-on supplementary packages that provide seamless functionality between design, engineering, and optimization from a product development standpoint. However, there is still a disconnect between research and practical industry in terms of specified tolerances by a designer versus achievable manufacturing tolerances as coupled to a cost trade-off model [38]. Additionally,

various robust methods' research lacks the connection with functional geometric dimensioning & tolerancing schemas which make for somewhat subpar optimization results.

Moreover, the assortment of robust design methods involving transmitted variation, Taguchi methods, stochastic optimization, etc., are not specifically clear in their usage from an overall systems procedural approach in terms of knowing which method is best to use and when, and whether combined methods would offer even greater insight for creating designs that are more optimally robust. Other issues such as those related to the method of transmitted variation include nonnormal distributions, correlated variables, higher order models, and other forms of uncertainty along with the potential lack of absolute surety in terms of local vs. global optimization convergence results within the design space. Multi-objective optimization certainly adds increasing complexity to the mix. Although correlation and higher order models have been developed, it is unsure as to the seamless integration between the various methods and their criteria of use. Consequently, there lies potential research in these areas. Exploring optimization through CAE software may provide more insight into this as companies such as OptiY/ANSYS have sophisticated optimization strategies for solving various robust design/robust design optimization problems.

Nevertheless, and although there have been recent advancements in research related to robust design in terms of Geometric Dimensioning & Tolerancing (GD&T) and taking a concurrent engineering approach, there still is a disconnect as to the development of a working systems engineering approach that takes into account all aspects of the value chain. It is proposed that the Design for Six Sigma (DFSS/DMADV) methodology is most aptly suited for this which links to robust design as per statistical tolerancing but with superimposed GD&T methods and coupled to manufacturing process capability thus closing the gap between design, manufacturing, and inspection from a functional perspective. Additionally, incorporating enterprise data management in conjunction to Artificial Intelligence/ Machine Learning (AI/ML) techniques and the digital twin would further integrate the DFSS process thus facilitating greater robustness from both a joined process and product scope in light of Industry 4.0.

Further research into all of these areas in concert may provide way for contributions in the robust design/robust design optimization arena. Notwithstanding, applicability of these methods, specifically to self-centering kinematic mechanisms design research, along with CAE integration will ensue as complimentary to the associated wedge cam and sensitivity robust design optimization procedures. Extending upon such, design tolerances linked with manufacturing process capability in conjunction to statistical tolerancing connected with feasibility robust design optimization will be incorporated in future research for further balancing and vibration minimization as well as true physical clamping is concerned. Following, physical prototypes of baseline concepts vs. optimized concepts along with experimental testing coupled with studies into the nonlinear dynamic re-

sponse of these cams subjected to rapid load changes, particularly relevant in robotics applications, in addition to reviewing how dynamic loads affect wear and longevity in relation to clamping accuracy will commence. In conjunction, this may be contained within the DFSS framework for taking a holistic systems engineering approach to robust design as it is almost always the case that a system vs. component view will produce the best design [39].

Authors' Contributions

Shawn P. Guillory: Conceptualization, Formal analysis, Methodology, Validation, Visualization, Writing-original draft, Writing-review & editing, **Alan A. Barhorst:** Supervision, Writing-review, **Jim Lee:** Writing-review, **Jonathan R. Raush:** Writing-review, **Raju Gottumukkala:** Writing-review, **Terrence L. Chambers:** Supervision, Writing-review.

Acknowledgments

The authors would like to provide a special note of appreciation toward Mr. Jason and Jacob Neu, both with Neu Company, LLC, a Civil/Structural Engineering firm specializing in the overhead crane, heavy industrial, oil & gas and maritime industries, for their industry support toward my professional career growth and family life during my doctoral studies which comprise this manuscript's research.

Conflicts of Interest

The authors declare no conflicts of interest regarding the publication of this paper.

References

[1] Bruno, D. (1970) Clamping Device. U.S. Patent No. 3535963.27.

[2] Dietmar, H. and Herbert, I. (1984) Steady for Holding Rod-Like Circular Cross-Section Components. U.S. Patent No. 4463635.07.

[3] Guy, W. (1989) Self-Centering Steady Rest. U.S. Patent No. 4823657.25.

[4] Karl, H. (1988) Self-Centering Steady Rest for Lathe. U.S. Patent No. 4754673 05.

[5] Paul, O. (1985) Multi-Purpose Steady Rest. U.S. Patent No. 4546681.15.

[6] Peter, F. (2002) Self-Centering Steady Rest Clamping Device. U.S. Patent No. 6458022.01.

[7] Peter, H. and Eckhard, M. (2011) Self-Centering Steady Rest. U.S. Patent No. 20110209591.01.

[8] Peter, H. and Eckhard, M. (2014) Self-Centering Steady Rest. U.S. Patent No. 8726772 B2.20.

[9] Richard, L. (2008) Steady Rest for Rotating Shaft. U.S. Patent No. 20080139092.12.

[10] Stefano, R. (1985) Selfcentering Work-Rest. U.S. Patent No. 4519279.28.

[11] ARMS Automation. https://www.armsautomation.com

[12] Arobotech Systems Inc. https://arobotech.com/

[13] Atling Steady Rest. https://www.atling.com/

[14] Fenwick and Ravi. https://www.fenwickandravi.co.in/

[15] Kitagawa. https://kitagawa.global/

[16] RÖHM (2024). http://www.roehm.biz/

[17] SAJRAJ Technologies. www.steadyrestmanufacturer.com/

[18] SCHUNK SE & Co. KG. https://www.schunk.com/

[19] SMW-AUTOBLOK. https://www.smwautoblok.com/

[20] David, S., Jeff, H., Lawrence, H. and Bernd, R. (2009) Positioning and Spinning Device. U.S Patent No. 7509722-B2.

[21] Afandiyev, E.M. and Nuriyev, M.N. (2021) Analysis of the Condition of a Pipe Fixed in a Clamping Device. *Eureka: Physics and Engineering*, No. 1, 78-85.

[22] Wang, L., Guo, S., Gong, H. and Shang, X. (2016) Research and Development of a Self-Centering Clamping Device for Deep-Water Multifunctional Pipeline Repair Machinery. *Natural Gas Industry B*, **3**, 82-89. https://doi.org/10.1016/j.ngib.2015.12.012

[23] Bavadekar, P.S., Survase, P.P., Hogade, R.S., Patil, S.R., Dhokale, O.S. and Mhamane, D.A. (2020) Design and Analysis of Self Centering Steady Rest for CNC Turning Machine. *International Research Journal of Engineering and Technology*, **6**, 13-21.

[24] Rajendra, B.L. and Satish, B.G. (2016) Design and Analysis of Self Centering Steady Rest for Supercut-6 CNC Turning Machine Using CAD & FEA. *Ram Meghe Institute of Technology & Research*, **4**, 14-19.

[25] Dinesh, J.G. and Pooja, J.S. (2015) Design and Analysis of Self Centering Automatic Gripper (Steady Rest) for Supercut-6 CNC Turning Machine Using CAD and FEA. *International Engineering Research Journal*, No. 2, 65-68.

[26] Chen, T.L. and Xie, Z.Q. (2019) Design and Machining of Translation Cam for Self-Centering Center Rest. *Mechanical Research & Application*, **32**, 152-154, 159.

[27] He, R.K. (1999) Cam Curve Design and Processing of Hydraulic Center Frame. *Machinery Design & Manufacture*, No. 4, 46.

[28] Li, J.R. (1991) Calculation of Working Wedge Curve of Self-Centering Steady Rest. *Modern Manufacturing Engineering*, No. 11, 27-28.

[29] Liu, B.F. and Xu, X.D. (2000) Solving the Translational Convex Contour of the Open Self-Centering Center Frame Using the Instantaneous Center Method. *Journal of Jiangnan University*, **15**, 34-37.

[30] Lu, X.Y. and Xie, N.B. (2008) Research on the Derivation of Cam Curve of Hydraulic Self-Centering Steady Rest. *Machinery Design & Manufacture*, No. 4, 24-25.

[31] Wang, Y.L. and Yin, Q.F. (2019) Design and Machining of Cam Curve of the Self-Centering Steady Rest. *Manufacturing Technology & Machine Tool*, No. 3, 64-66.

[32] Xiao, K. (2013) Calculation of Internal Process Cam Curve of Self-Centering Steady Rest. *Equipment Manufacturing Technology*, No. 3, 149-150.

[33] Xu, N.N. and Tang, W.C. (2015) Design Calculation for Wedge Cam of Small Roller Centering Three-Jaw Jig. *Key Engineering Materials*, **656**, 641-645. https://doi.org/10.4028/www.scientific.net/kem.656-657.641

[34] Xie, Z.Q. (2021) Design and Machining of Self-Centering Center Rest Cam Mechanism Based on Linear Approximation. *Mechanical Research and Application*, 34, 77-82.

[35] Zuqiang, X., Yong, N. and Qiulian, M. (2021) Research on Linear Approximation of Errors Such as Convex Contour Line of Self-Centering Steady Frame. *Mechanical*

Engineering and Automation, No. 2, 34-39.

[36] Zhao, Y.Q., Wang, Y.F. and Hou, H.L. (2016) Mechanism Design and Optimization of Self-Centering Steady Rest Used in Grinding Machine. China Mechanical Engineering, **27**, 2322-2327.

[37] Guillory, S.P., Barhorst, A.A., Lee, J., Gottumukkala, R., Raush, J.R. and Chambers, T.L. (2025) Generalized Robust Systems-Based Theoretical Kinematic Inverse/Regular Wedge Cam Theory for Three-Point Diametral Self-Centering Motion. *Journal of Applied Mathematics and Physics*, **13**, 729-796. https://doi.org/10.4236/jamp.2025.133040

[38] Parkinson, A. (1995) Robust Mechanical Design Using Engineering Models. *Journal of Mechanical Design*, **117**, 48-54. https://doi.org/10.1115/1.2836470

[39] Parkinson, A.R., Hedengren, J.D. and Balling, R.J. (2013) Optimization Methods for Engineering Design. Applications and Theory, Brigham Young University.